Surfaces and Interfaces 25 (2021) 101267

Contents lists available at ScienceDirect

Surfaces and Interfaces

journal homepage: www.sciencedirect.com/journal/surfaces-and-interfaces

Significance of multiple slip and nanoparticle shape on stagnation point flow of silver-blood nanofluid in the presence of induced magnetic field

Alphonsa Mathew [a,*], Sujesh Areekara [a], A.S. Sabu [a], S. Saleem [b]

[a] Department of Mathematics, St. Thomas' College (Autonomous), Thrissur 680001, Kerala, India
[b] Department of Mathematics, College of Sciences, King Khalid University, Abha 61413, Saudi Arabia

ARTICLE INFO

Keywords:
Nanoparticle shape effect
Induced magnetic field
Stagnation point flow
Multiple slip effect
Linear heat source
Thermal radiation

ABSTRACT

Non-spherical nanoparticles have gained popularity for their ability in changing the thermophysical properties of a nanofluid. The current work focuses on studying the significance of multiple slip and nanoparticle shape on stagnation point flow of blood-based silver nanofluid considering chemical reaction, induced magnetic field, thermal radiation, and linear heat source which is beneficial in cancer therapy, biomedical imaging, hyperthermia, and tumor therapy. Relevant similarity transformations are effectuated in converting the mathematically modeled governing equations into a system of ODEs and are then numerically resolved in MATLAB employing the adaptive Runge-Kutta method and the Newton Raphson method. Observations on the consequence of differing parameters on varying attributes are achieved via tables and graphs. Additionally, the shape effect of nanoparticles on various attributes is also evaluated. Linear heat source and thermal radiation parameters exhibit a constructive effect whereas the thermal slip parameter exhibits a destructive effect on temperature. Further, it is observed that the blade-shaped nanoparticle exhibits the greatest heat transfer rate followed by platelet, cylinder, and spherical-shaped nanoparticles, respectively.

1. Introduction

Nanofluid, discovered by Choi and Eastman [1], was known for its unparalleled heat transfer and cooling abilities. Choi proposed nanofluid as a suspension of nanoparticles (1–100 nm in size) and observed that the conventional fluid and nanofluid exhibit distinct physical and chemical properties. According to Ying-Qing et al. [2] and Oke et al. [3], the inherent nature of nanoparticles is bound to affect the temperature distribution. Neethu et al. [4] investigated the significance of the nanoparticle volume fraction on the hydromagnetic flow between two vertical porous plates moving in opposite directions based on the single-phase nanofluid model proposed by Tiwari and Das [5]. They observed a decline in the nanoliquid temperature profile due to augmenting nanoparticle volume fraction. However, augmenting nanoparticle volume fraction tends to increase the nanoliquid temperature in an unsteady nanoliquid flow past an inclined plate (see Mackolil and Mahanthesh [6]). A few studies exploring nanofluid flow can be seen in [7–11].

Particles of silver between 1 and 100 nm, called silver nanoparticles, have been proved to be beneficial in the medical field with their antibacterial properties and also due to their applicability in the treatment of many diseases; namely cancer (see [12–14]). Abbasi et al. [15] examined the peristaltic transport of silver-water nanofluid in the presence of constant applied magnetic field considering Ohmic heating, velocity slip, thermal slip, and Hall effects. They observed that the addition of 5% silver nanoparticles reduced the velocity and temperature of the base fluid by 10% and 16%, respectively. The dominating nature of silver nanoliquid over copper nanoliquid on the heat transfer rate was observed by Hayat et al. [16] and Sravanthi [17]. In addition, Hayat et al. [18] noted that the Bejan number is more for Ag-water nanofluid. The increment of the average Nusselt number by increasing the volume fraction of nanoparticles for typical nanofluid is more sensible than hybrid nanofluid in an enclosure with rotating heat sources (see Jamiaita [19]). The study on the hydrothermal and irreversibility behaviour of a biologically synthesized silver-water nanoliquid in a wavy microchannel heat sink, conducted by Al-Rashed et al. [20], revealed that the nanoliquid has a better cooling performance in comparison with pure water.

The nanoparticles can be categorized into spherical and non-spherical nanoparticles based on their physical shape. Different shaped nanoparticle exhibits different properties and different heat transfer capabilities (see Truong et al. [21]). Timofeeva et al. [22] analyzed the thermophysical properties of alumina nanofluid with different nanoparticle shapes; namely platelet, blade, brick, and cylinder; both practically and theoretically. Ellahi et al. [23] pointed out that the lowest

* Corresponding author.
E-mail address: alphonsa@stthomas.ac.in (A. Mathew).

https://doi.org/10.1016/j.surfin.2021.101267
Received 2 April 2021; Received in revised form 26 May 2021; Accepted 3 June 2021
Available online 10 June 2021
2468-0230/

Nomenclature

a, c	Dimensional constants
D_B	Mass diffusivity (m^2s^{-1})
k_r	Reaction rate constant(s^{-1})
C_{slip}	Solutal slip parameter
C	Fluid concentration
T	Fluid temperature (K)
C_W	Nanoparticle concentration near the wall
T_W	Wall fluid temperature
Cf_x	Local drag coefficient
q_T	Heat source coefficient
Pr	Prandtl number
q_r	Radiative heat flux
Kr	Chemical reaction parameter
N_1	Temperature slip factor
C_p	Specific heat
u, v	Velocity components (ms^{-1})
M_0	Uniform magnetic field at infinity (Am^{-1})
T_∞	Ambient fluid temperature
T_{slip}	Thermal slip parameter
k^*	Mean absorption coefficient
Q_T	Linear heat source
N_2	Concentration slip factor
M_e	Magnetic field at free stream
R_d	Thermal radiation parameter
Sh_x	Local Sherwood number
Nu_x	Local Nusselt number
Re_x	Local Reynolds number
x, y	Cartesian coordinates(m)
C_∞	ambient nanoparticle concentration
Le	Lewis number

Greek symbols

ϑ	Kinematic viscosity (m^2s^{-1})
η	Dimensionless variable
σ^*	Stefan- Boltzmann constant
λ	Reciprocal of magnetic Prandtl number
α_m	Magnetic diffusivity (m^2s^{-1})
ϕ	Nanoparticle volume fraction
ρ	Density of the fluid (kgm^{-3})
κ	Thermal conductivity ($Wm^{-1}K^{-1}$)
μ_e	Magnetic permeability ($kgms^{-2}A^{-2}$)
σ	Electrical conductivity ($kg^{-1}m^{-3}s^3A^2$)
β	Magnetic parameter
α	Thermal diffusivity (m^2s^{-1})

Subscripts

nf	Nanofluid
f	Conventional fluid

velocity and highest temperature of the nanoliquid were caused by the sphere and disc-shaped particles, respectively for the mixed convective nanoliquid flow past a vertical lengthening permeable sheet. In addition, Benkhedda et al. [24] reported that the maximum friction factor is exhibited by the platelet-shaped silver-titanium dioxide nanoparticles. The reduction in the temperature profile of $Cu - CuO/$blood with the increasing shape factor values was revealed by Tripathi et al. [25]. A comparative analysis of $Ti - H_2O$and$Ag - H_2O$nanofluids on the effect of nanoparticle shape in a microchannel, conducted by Sindhu and Gireesha [26], showcased that the silver nanofluid exhibited higher entropy than the titanium nanofluid. They also observed that the entropy generation is high in the case of disc-shaped nanoparticles, followed by needle and sphere-shaped nanoparticles. Recently, Elnaqeeb et al. [27] investigated the dynamics of water conveying nanoparticles with various densities and shapes through a rectangular closed domain and observed that the heat transfer is maximal in the case of ternary-hybrid nanofluid made up of copper oxide, copper, and silver nanoparticles.

Blood is a connective tissue in fluid form (see Sembulingam and Sembulingam [28]). Blood flow utilizing nanoparticles are important in the medical industry for cancer treatment and drug delivery. The significance of partial slip and buoyancy on the blood-gold Carreau nanofluid flow over an upper horizontal surface of a paraboloid of revolution was investigated by Koriko et al. [29]. They observed that the maximum values for surface drag and the heat transfer rate was showcased by smaller values of Deborah number. The augmentation in the volume fraction of carbon nanotubes increased the blood temperature (see Khalid et al. [30]). Dinarvand et al. [31] pointed out that the use of CuOandCu hybrid nanoparticles reduced the haemodynamic effect of the capillary relative to the pure blood case. In addition, Khan et al. [32] numerically simulated the nonlinear radiative flow of Casson gold-nanoliquid through a stretched rotating rigid disk subject to Lorentz force utilizing the three-stage Lobatto method. Recently, Ashraf et al. [33] utilized the generalized differential quadrature method to explore the peristaltic flow of blood-based Casson nanomaterial containing platelet-shaped magnetite nanoparticles. Further, the significance of partial slip due to lateral velocity and viscous dissipation for blood-gold Carreau nanomaterial and dusty fluid was elucidated by Koriko et al. [34]. A significant difference in the effect of partial slip on the dynamics of dusty fluid and blood-gold nanomaterial was observed.

Induced magnetic field (IMF) is the additional magnetic field that gets induced on electrically conducting fluid in the presence of an external magnetic field. This phenomenon is due to the impact of a larger magnetic Reynolds number. IMF has applications in MRI, glass manufacturing, geophysics, and MHD generators, etc. IMF paired with blood flow plays a decisive role in blood pumps, treatment of cardiac diseases and has many other biomedical applications. Kumari et al. [35] explored the flow and heat transfer of an electrically conducting fluid (which is at rest) over an elongating sheet in the presence of sources/-sinks and induced magnetic field. Later, the MHD flow over a lengthening sheet in the presence of an induced magnetic field was reinvestigated by Ali et al. [36]. Iqbal et al. [37] scrutinized the influence of induced magnetic field on ferrofluid past a vertical stretching surface and observed that velocity profile enhanced for assisting flow with magnetic parameter. Gireesha et al. [38] numerically analyzed nanofluid stagnation point flow past a stretching surface attending IMF and found out that the induced magnetic field enhances with the intensifying hydromagnetic field. Iqbal et al. [39] elucidated the influence of induced magnetic fields on water-based copper and titanium dioxide nanofluids utilizing the Keller box method. An opposite relation was found to exist between magnetic parameter and temperature profile. Further, Amjad et al. [40] studied the influence of Lorentz force and induced magnetic field on Casson micropolar nanoliquid over a permeable curved stretching/shrinking surface.

Regarding stagnation point flow, the velocity of the fluid at the striking point of the rigid body is zero. It proposes many applications in engineering, industry, and physiological fluid flows. Ali et al. [41] extended the work of Mahapatra and Gupta [42] to analyze the hydromagnetic stagnation point flow of an electrically conducting fluid over a lengthening sheet in the presence of an induced magnetic field. Later, Junoh et al. [43] extended the work of Ali et al. [41] by considering the stagnation point flow past a stretching/shrinking sheet in a hybrid nanomaterial. Abbas et al. [44] explored the stagnation-point hybrid nanofluid flow over a slip surface. They adopted the Runge-Kutta-Fehlberg method to numerically solve the nonlinear system of differential equations and

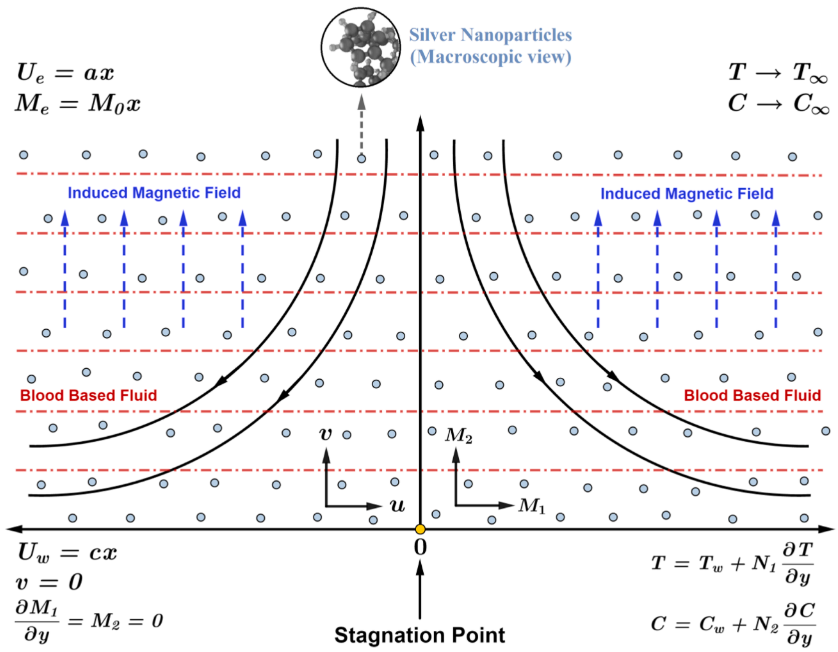

Fig. 1. Figurative representation.

Table 1

Comparison of drag coefficient ($Cf_x\, Re_x^{1/2}$) with [47,62,63] for different A values when $\phi = \beta = 0$.

A	$Cf_x\, Re_x^{1/2}$			
	Iqbal et al. [47]	Hayat et al. [62]	Hayat et al. [63]	Present study
0.1	−0.969386	−0.96939	−0.96937	−0.9693861
0.2	−0.918107	−0.91811	−0.91813	−0.9181071
0.5	−0.667263	−0.66726	−0.66723	−0.6672637
0.7	−0.433475	−0.43346	−0.43345	−0.4334756
0.8	−0.299388	−0.29929	−0.29921	−0.2993888
0.9	−0.154716	−0.15458	−0.1545471	−0.1547167
1	0	0	0	0

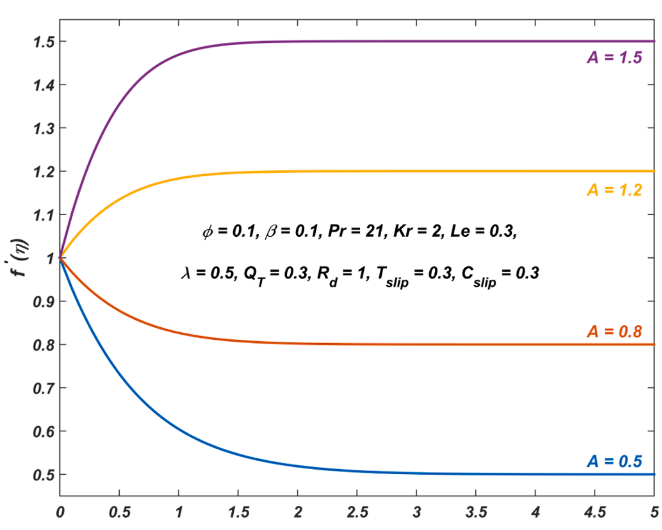

Fig. 2. $f'(\eta)$ for differing A values.

noted that the velocity is inversely proportional to the velocity ratio parameter. Al-Amri and Muthtamilselvan [45] investigated stagnation point nanofluid flow containing micro-organisms and found an enhanced

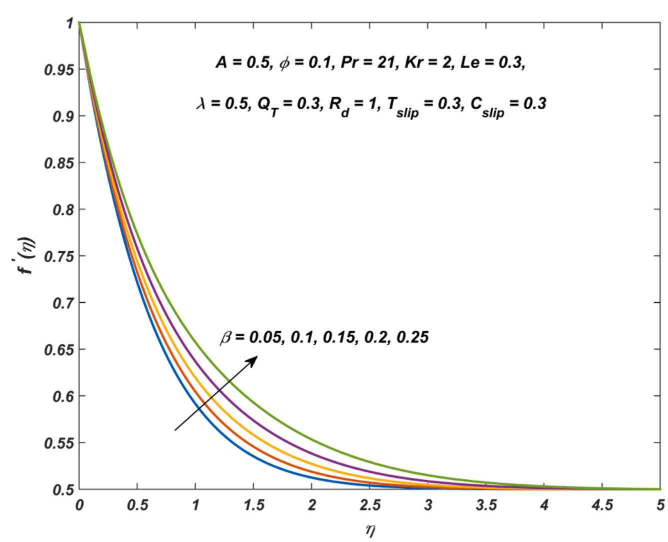

Fig. 3. $f'(\eta)$ for differing β values.

velocity profile due to augmenting stagnation parameter. Some other studies concerning stagnation point flow can be seen in [46–49].

The slip boundary condition characterizes the relative movement of fluid with the boundary. Multiple slip corresponds to the case when more than one slip (velocity, thermal, or solutal) condition is considered. Daniel et al. [50] reported that the augmenting velocity slip parameter slows the velocity profile. Khan et al. [51] and Amanulla et al. [52] noted that multiple slip effects have a positive impact on boundary layer flow. The decrease in the heat transfer rate due to the velocity slip parameter was observed by Ibrahim and Negera [53]. Further, a decrease in the temperature and concentration profile was noted due to the increased thermal and solutal slip parameter values, respectively (see Barik et al. [54]). A few studies discussing the slip effects can be seen in [55–58].

Motivated by the above-mentioned studies, it is noted that the effect of multiple slip, spherical and non-spherical (cylinder, platelet, and blade) nanoparticles on the stagnation point flow of silver-blood

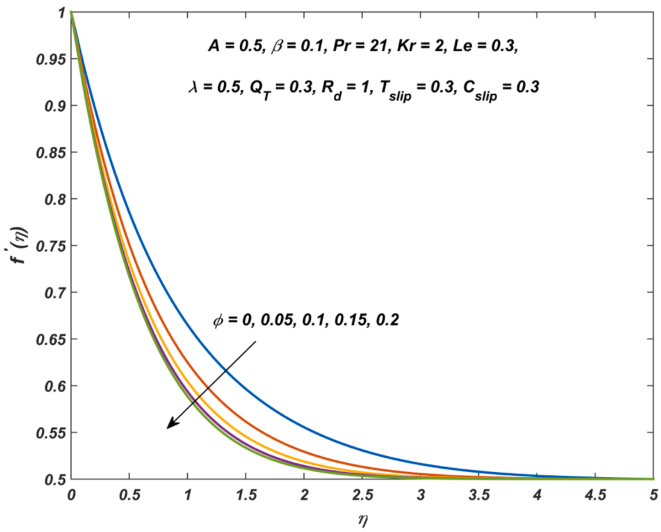

Fig. 4. $f'(\eta)$ for differing ϕ values.

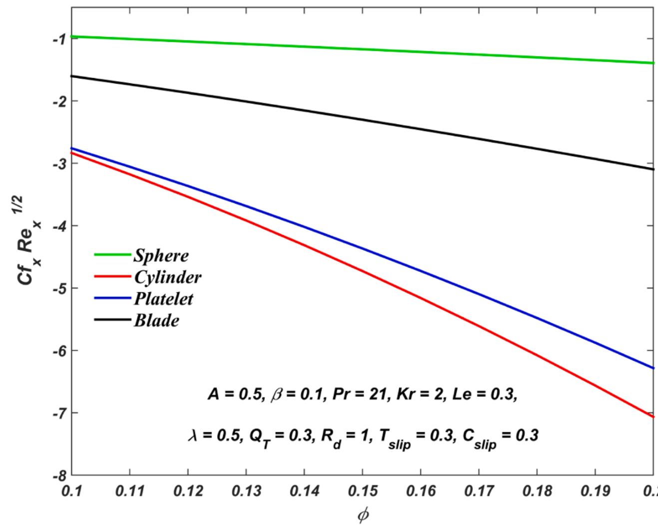

Fig. 7. $Cf_x\ Re_x^{1/2}$ for differing nanoparticle shapes and ϕ values.

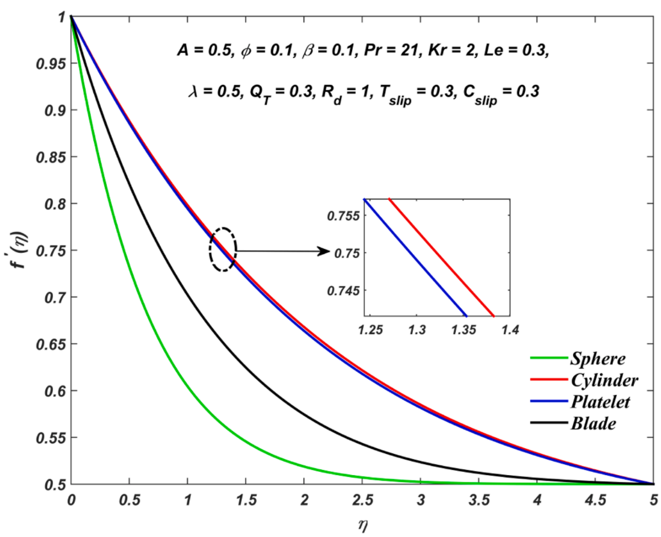

Fig. 5. $f'(\eta)$ for differing nanoparticle shapes.

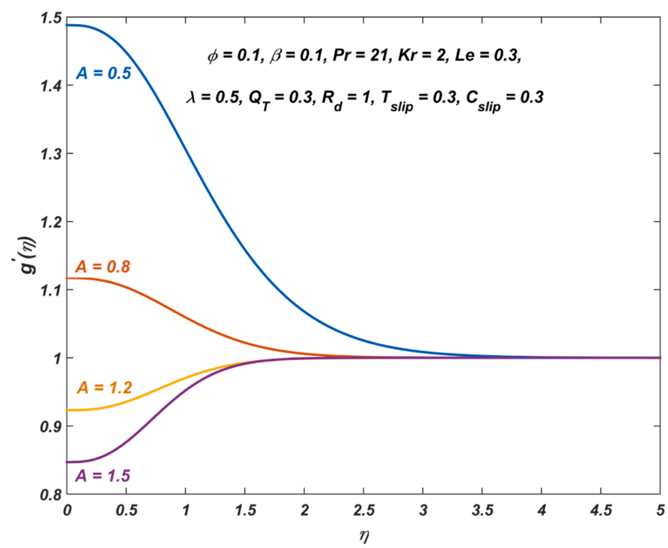

Fig. 8. $g'(\eta)$ for differing A values.

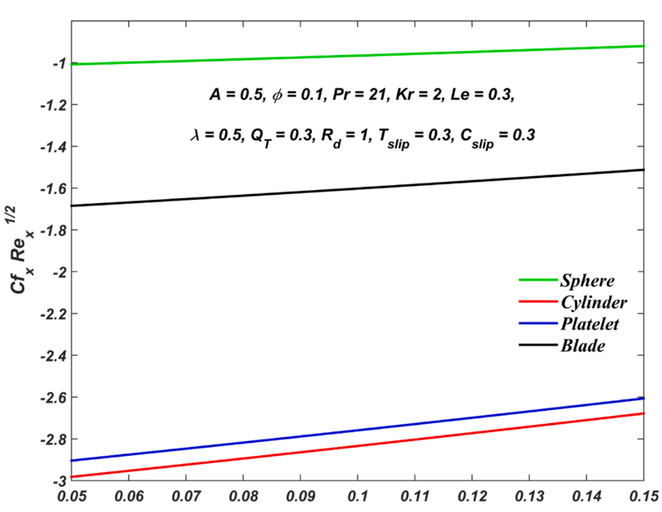

Fig. 6. $Cf_x\ Re_x^{1/2}$ for differing nanoparticle shapes and β values.

nanofluid in the presence of an induced magnetic field has not yet been studied. This paper attempts to fill this gap. In addition, linear heat source, chemical reaction and thermal radiation effects are incorporated. Further, thermal and solutal slip effects are also considered for a realistic approach. The present study has applications in cancer therapy, biomedical imaging, hyperthermia, and tumor therapy (see [21, 59–61]). The impact of pertinent parameters on the flow profiles has been analyzed with an emphasis on the following research questions:

- What is the significance of thermal slip and solutal slip parameters on the nanofluid temperature and nanofluid concentration, respectively?
- How does the nanoparticle shape affect the flow profiles?
- What is the variation in the nanofluid temperature with linear heat source, thermal radiation, and volume fraction of silver nanoparticles?
- How sensitive are the physical quantities with spherical and non-spherical nanoparticles?

2. Problem statement

Two-dimensional steady stagnation point flow over a linearly elongating sheet (Fig. 1) is considered under the ensuing assumptions:

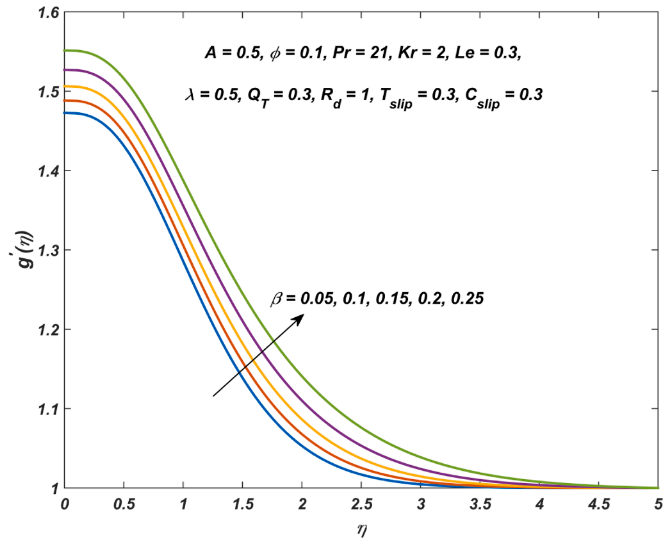

Fig. 9. $g'(\eta)$ for differing β values.

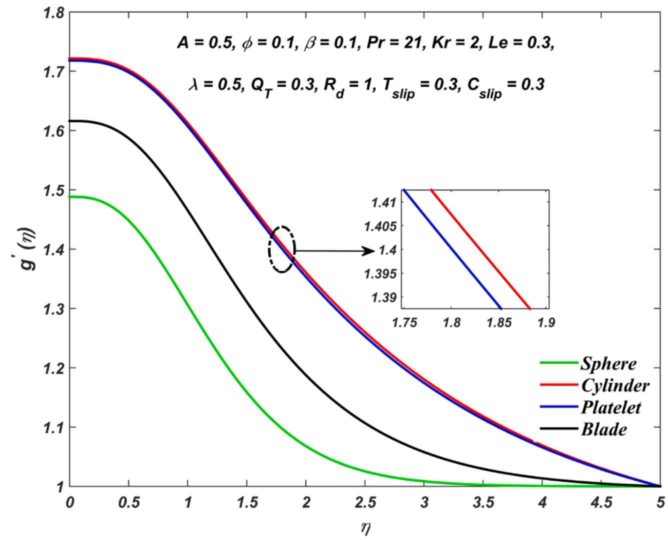

Fig. 11. $g'(\eta)$ for differing nanoparticle shapes.

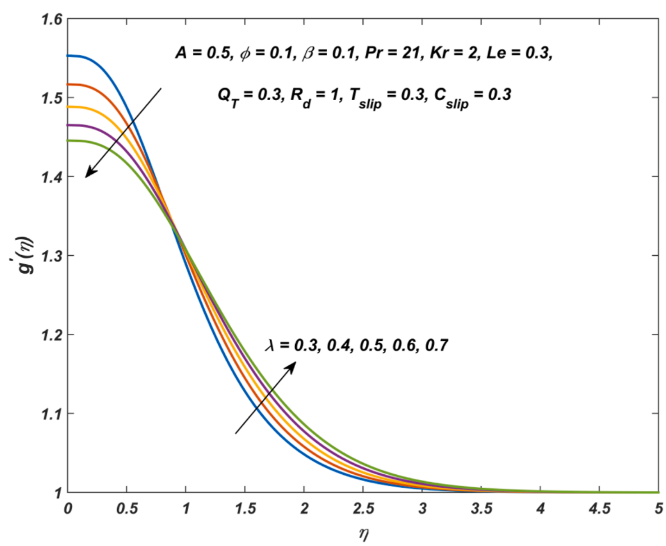

Fig. 10. $g'(\eta)$ for differing λ values.

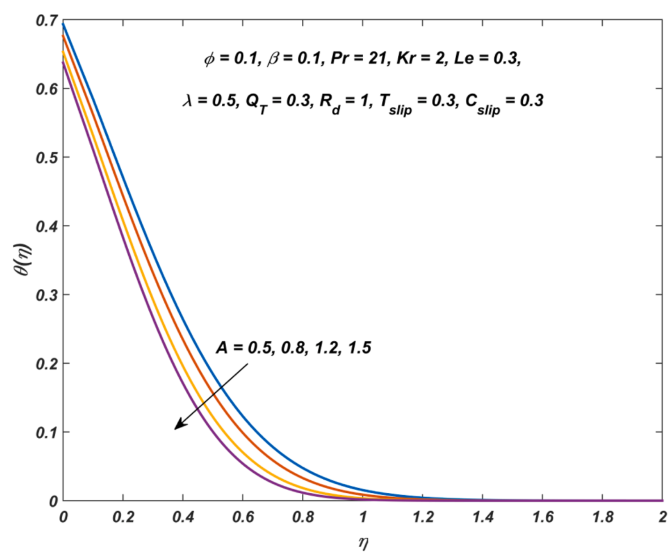

Fig. 12. $\theta(\eta)$ for differing A values.

(i) The expanding sheet is positioned along *xaxis* and blood-based silver nanofluid occupies the region$y > 0$.
(ii) $U_w(x) = cx$ and $U_e(x) = ax$ corresponds to the velocity of the lengthening sheet and the free stream, respectively.
(iii) Induced magnetic field vector, $M = (M_1, M_2)$ is considered with M_1 & M_2 being the magnetic integrants along x and y direction, respectively.
(iv) Chemical reaction, linear heat source, thermal radiation, and nanoparticle shape (sphere, cylinder, platelet, and blade) effects are incorporated.
(v) Thermal and solutal slip effects are also considered.

Governing equations [46–48,54] takes the form:

$$\frac{\partial u}{\partial x} + \frac{\partial v}{\partial y} = 0 \tag{1}$$

$$\frac{\partial M_1}{\partial x} + \frac{\partial M_2}{\partial y} = 0 \tag{2}$$

$$u\frac{\partial u}{\partial x} + v\frac{\partial u}{\partial y} - \frac{\mu_e}{4\pi\rho_{nf}}\left(M_1\frac{\partial M_1}{\partial x} + M_2\frac{\partial M_1}{\partial y}\right) = U_e\frac{dU_e}{dx} - \frac{\mu_e M_e}{4\pi\rho_{nf}}\frac{dM_e}{dx} + \left(\frac{\mu_{nf}}{\rho_{nf}}\right)\frac{\partial^2 u}{\partial y^2} \tag{3}$$

$$u\frac{\partial M_1}{\partial x} + v\frac{\partial M_1}{\partial y} - M_1\frac{\partial u}{\partial x} - M_2\frac{\partial u}{\partial y} = \alpha_m\frac{\partial^2 M_1}{\partial y^2} \tag{4}$$

$$u\frac{\partial T}{\partial x} + v\frac{\partial \mathrm{T}}{\partial y} = \alpha_{nf}\frac{\partial^2 \mathrm{T}}{\partial y^2} + \frac{q_T}{(\rho C_p)_{nf}}(T - T_\infty) - \frac{1}{(\rho C_p)_{nf}}\frac{\partial q_r}{\partial y} \tag{5}$$

$$u\frac{\partial C}{\partial x} + v\frac{\partial C}{\partial y} = D_B\frac{\partial^2 C}{\partial y^2} - k_r(C - C_\infty) \tag{6}$$

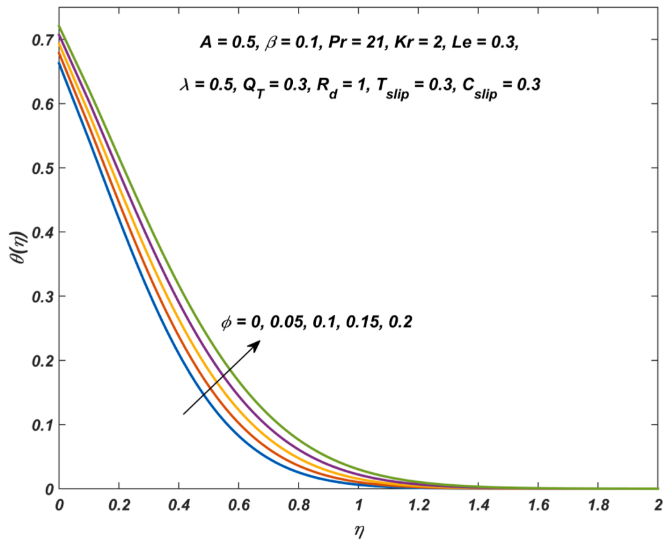

Fig. 13. $\theta(\eta)$ for differing ϕ values.

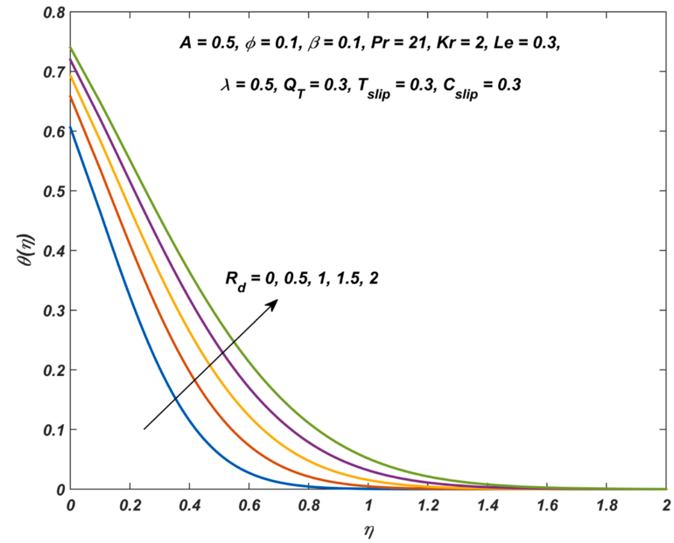

Fig. 15. $\theta(\eta)$ for differing R_d values.

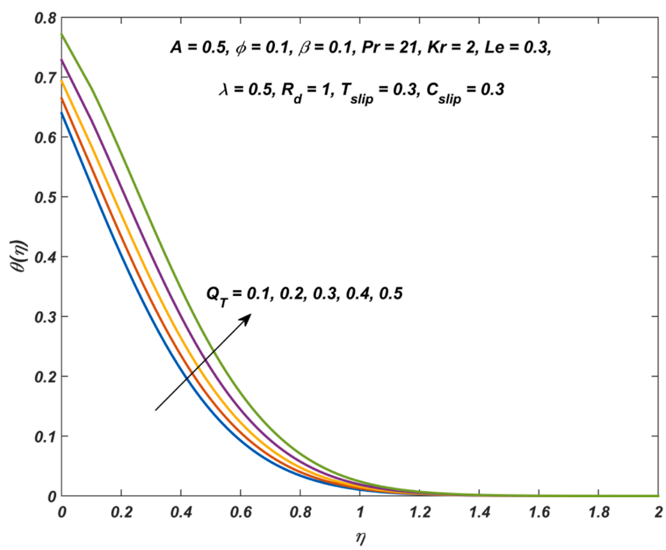

Fig. 14. $\theta(\eta)$ for differing Q_T values.

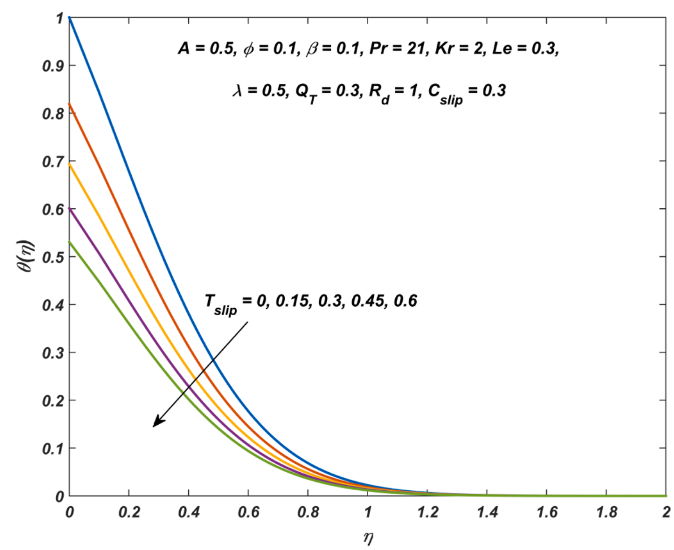

Fig. 16. $\theta(\eta)$ for differing T_{slip} values.

with

$$u = U_w(x) = cx,\ \ v = 0,\ \ \frac{\partial M_1}{\partial y} = M_2 = 0,\ \ \mathrm{T} = \mathrm{T}_w + N_1\frac{\partial T}{\partial y},\ \ C = C_w + N_2\frac{\partial C}{\partial y};\ \ at\ y = 0$$

$$u \rightarrow U_e(x) = ax, M_1 \rightarrow M_e(x) = M_0 x,\ \ \mathrm{T} \rightarrow \mathrm{T}_\infty,\ \ C \rightarrow C_\infty;\ as\ y \rightarrow \infty$$

where $\alpha_m = \frac{1}{4\pi\mu_e\sigma_{nf}}$ represents the magnetic diffusivity.

Introducing the following similarity transformations:

$$u = cxf'(\eta),\ \ v = -\sqrt{c\vartheta_f}f(\eta),\ \ M_1 = M_0 x g'(\eta),\ \ M_2 = -M_0\sqrt{\frac{\vartheta_f}{c}}g(\eta),$$

$$\eta = y\sqrt{\frac{c}{\vartheta_f}},\ \ \theta(\eta) = \frac{T - T_\infty}{T_w - T_\infty},\ \ \psi(\eta) = \frac{C - C_\infty}{C_w - C_\infty}\ .$$

and applying linearized Roseland approximation in equations (1) − (6), we get:

$$f''' = A_1\ A_2 \left\{ \ (f')^2 - f\,f'' - A^2 - \frac{\beta}{A_2}\ \{(g')^2 - g\ g'' - 1\} \ \right\} \tag{7}$$

$$g''' = \frac{A_5}{\lambda}\ \{\ g\,f'' - f\ g''\ \} \tag{8}$$

$$\theta'' = \frac{-Pr\ \{\ A_3\,f\ \theta' + Q_T\ \theta\ \}}{A_4 + \frac{4}{3}R_d} \tag{9}$$

$$\psi'' = Kr\ Le\ \psi - Le\ f\ \psi' \tag{10}$$

subject to the boundary conditions

$$f(0) = 0, f'(0) = 1,\ \ g(0) = 0,\ \ g''(0) = 0,\ \ \theta(0) = 1 + T_{slip}\ \theta'(0),\ \ \psi(0) = 1 + C_{slip}\ \psi'(0).$$

$$f'(\infty) \rightarrow A,\ \ g'(\infty) \rightarrow 1,\ \ \theta(\infty) \rightarrow 0,\ \ \psi(\infty) \rightarrow 0.$$

where the dimensionless parameters are :

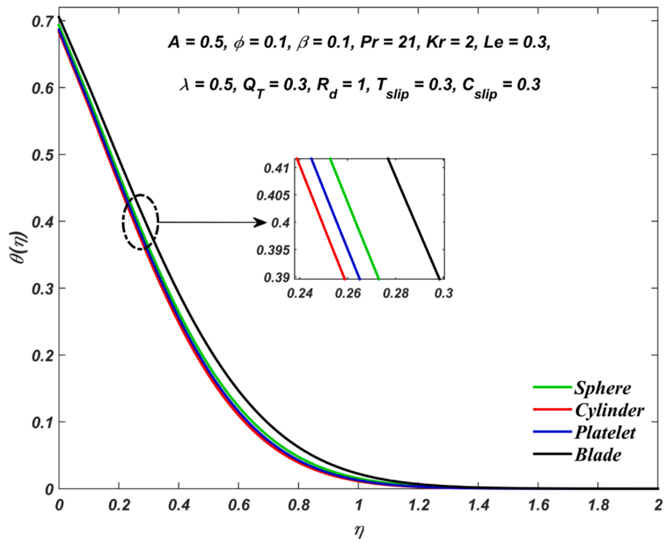

Fig. 17. $\theta(\eta)$ for differing nanoparticle shapes.

Table 2
Thermophysical properties [16,30,31] of blood and silver.

Property	Blood *(base fluid)*	Silver *(nanoparticle)*
ρ	1063	10490
C_p	3594	235
κ	0.492	429
σ	0.8	63 * 10^7

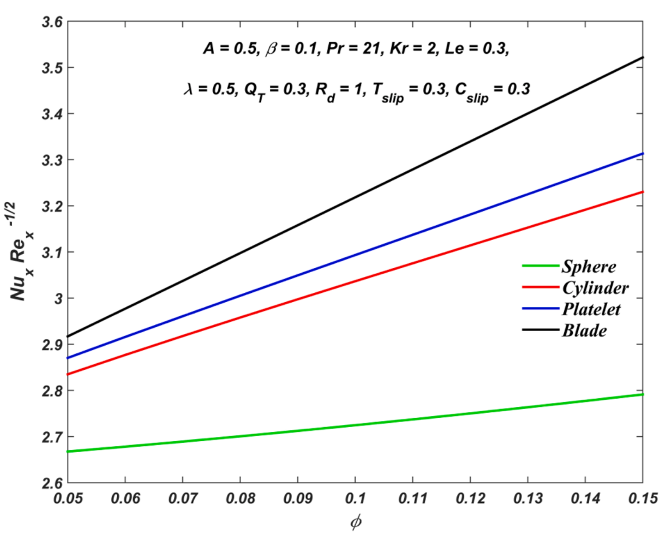

Fig. 18. $Nu_x\ Re_x^{-1/2}$ for differing nanoparticle shapes and ϕ values.

$$A = \frac{a}{c},\ \beta = \frac{\mu_e}{4\ \pi\ \rho_f}\left(\frac{M_0}{c}\right)^2,\ \lambda = \frac{1}{4\ \pi\ \mu_e\ \sigma_f\ \vartheta_f},\ Pr = \frac{(\mu C_p)_f}{\kappa_f},\ R_d = \frac{4\ \sigma^*\ {T_\infty}^3}{k^*\ \kappa_f},$$

$$Q_T = \frac{q_T}{c\ (\rho C_p)_f},\ Kr = \frac{k_r}{c},\ Le = \frac{\vartheta_f}{D_B},\ T_{slip} = N_1\sqrt{\frac{c}{\vartheta_f}},\ C_{slip} = N_2\sqrt{\frac{c}{\vartheta_f}}.$$

The nanofluid models [24] incorporated are :

Spherical	*Non-spherical*
$\frac{\mu_{nf}}{\mu_f} = \frac{1}{(1-\phi)^{2.5}} = \frac{1}{A_1}$	$\frac{\mu_{nf}}{\mu_f} = 1 + A_{shape}\ \phi + B_{shape}\ \phi^2 = \frac{1}{A_1}$

(*continued on next column*)

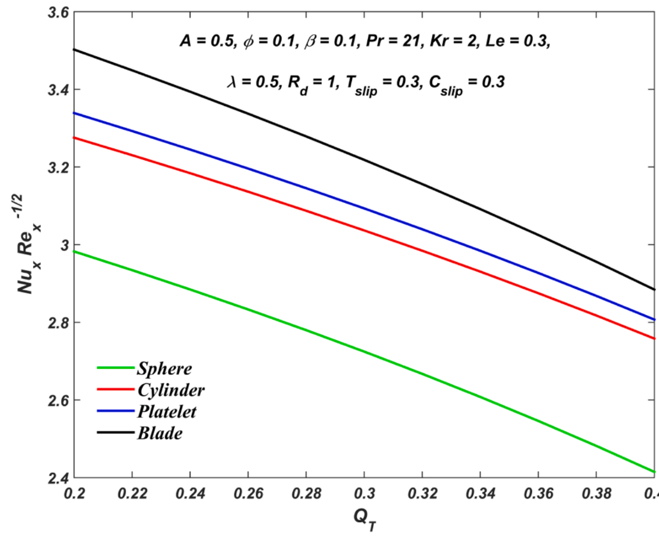

Fig. 19. $Nu_x\ Re_x^{-1/2}$ for differing nanoparticle shapes and Q_T values.

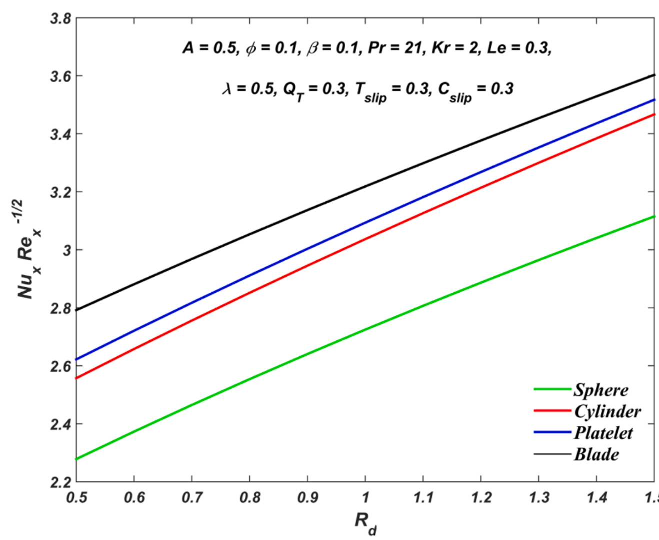

Fig. 20. $Nu_x\ Re_x^{-1/2}$ for differing nanoparticle shapes and R_d values.

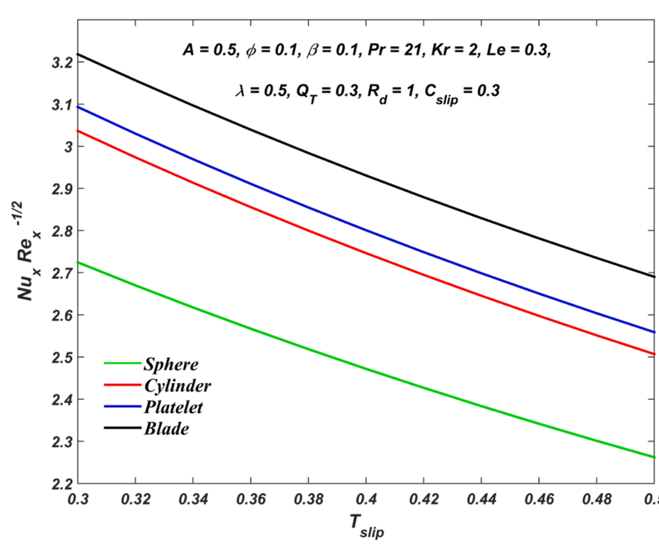

Fig. 21. $Nu_x\ Re_x^{-1/2}$ for differing nanoparticle shapes and T_{slip} values.

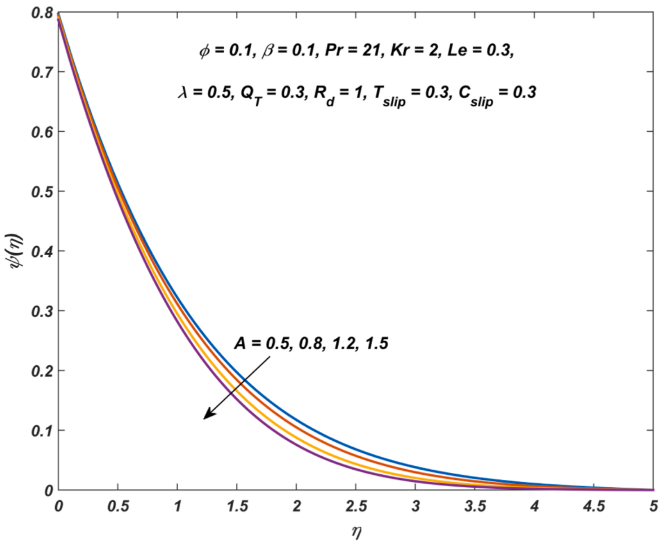

Fig. 22. $\psi(\eta)$ for differing $\boldsymbol{A}$ values.

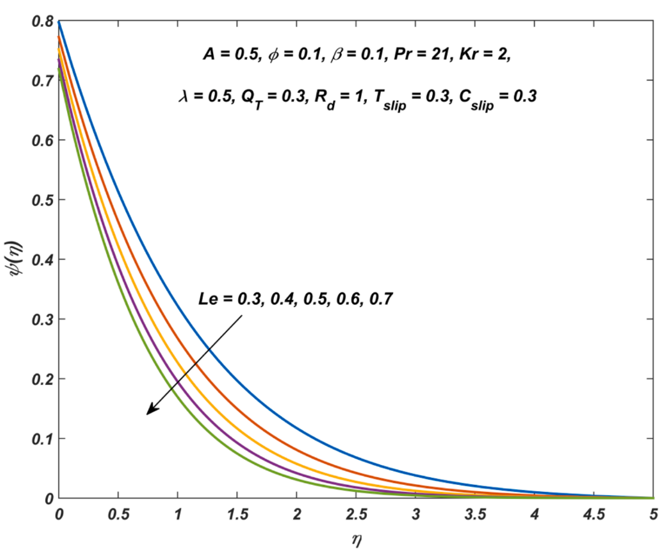

Fig. 23. $\psi(\eta)$ for differing $\boldsymbol{Le}$ values.

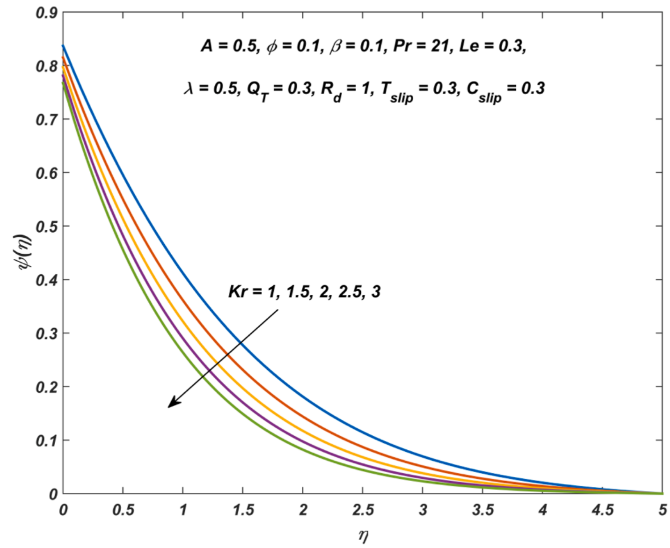

Fig. 24. $\psi(\eta)$ for differing $\boldsymbol{Kr}$ values.

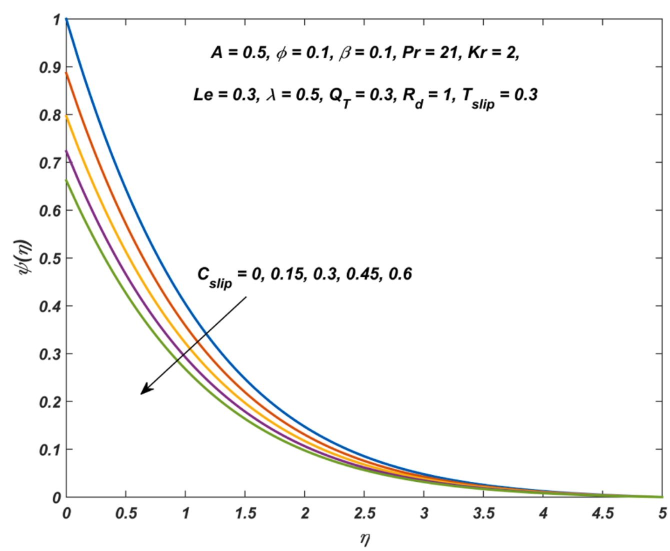

Fig. 25. $\psi(\eta)$ for differing $\boldsymbol{C_{slip}}$ values.

(*continued*)

Spherical	*Non-spherical*
$A_2 = \frac{\rho_{nf}}{\rho_f} = (1-\phi) + \phi\left(\frac{\rho_{Ag}}{\rho_f}\right)$	
$A_3 = \frac{(\rho C_p)_{nf}}{(\rho C_p)_f} = (1-\phi) + \phi\left(\frac{(\rho C_p)_{Ag}}{(\rho C_p)_f}\right)$	
$A_4 = \frac{\kappa_{nf}}{\kappa_f} = \frac{\kappa_{Ag} + (s-1)\kappa_f - (s-1)\phi(\kappa_f - \kappa_{Ag})}{\kappa_{Ag} + (s-1)\kappa_f + \phi(\kappa_f - \kappa_{Ag})}$	
$A_5 = \frac{\sigma_{nf}}{\sigma_f} = 1 + \frac{3\left(\frac{\sigma_{Ag}}{\sigma_f} - 1\right)\phi}{\left(\frac{\sigma_{Ag}}{\sigma_f} + 2\right) - \left(\frac{\sigma_{Ag}}{\sigma_f} - 1\right)\phi}$	

The nanoparticle shape properties [24] are:

	Sphere	*Cylinder*	*Platelet*	*Blade*
$\boldsymbol{A_{shape}}$	-	13.5	37.1	14.6
$\boldsymbol{B_{shape}}$	-	904.4	612.6	123.3
Shape factor, $\boldsymbol{s}$	3	4.9	5.7	8.6

Table 3
Variation in $Sh_x\ Re_x^{-1/2}$ when $A = 0.5,\ \beta = 0.1,\ \lambda = 0.5\ \&\ \phi = 0.1$.

Kr	*Le*	C_{slip}	$Sh_x\ Re_x^{-1/2}$			
			Sphere	*Cylinder*	*Platelet*	*Blade*
1.5	0.3	0.3	0.6166	0.6263	0.6261	0.6217
2			0.6773	0.6852	0.6850	0.6815
2.5			0.7298	0.7363	0.7362	0.7333
2	0.2	0.3	0.5737	0.5808	0.5807	0.5774
	0.3		0.6773	0.6852	0.6850	0.6815
	0.4		0.7594	0.7675	0.7674	0.7638
2	0.3	0.2	0.7265	0.7355	0.7354	0.7313
		0.3	0.6773	0.6852	0.6850	0.6815
		0.4	0.6343	0.6412	0.6411	0.6380

Physical quantities [47,49] (in dimensionless form) are given by:

Local drag coefficient :	$Cf_x = \dfrac{\tau_\omega}{\rho_f\ (U_W)^2} = \dfrac{\mu_{nf}\ \frac{\partial u}{\partial y}\|_{y=0}}{\rho_f\ (U_W)^2} \Rightarrow Cf_x\ Re_x^{1/2} = \dfrac{f''(0)}{A_1}.$
Local Nusselt number :	$Nu_x = \dfrac{x\ q_\omega}{\kappa_f\ (T_W - T_\infty)} = \dfrac{-x\left(\kappa_{nf}\frac{\partial T}{\partial y} - q_r\right)\|_{y=0}}{\kappa_f\ (T_W - T_\infty)} \Rightarrow Nu_x\ Re_x^{-\ 1/2} = -\left(A_4 + \frac{4}{3}R_d\right)\ \theta'(0)\ .$
Local Sherwood number :	$Sh_x = \dfrac{x\ q_m}{D_B\ (C_W - C_\infty)} = \dfrac{-x\ D_B\ \frac{\partial C}{\partial y}\|_{y=0}}{D_B\ (C_W - C_\infty)} \Rightarrow Sh_x\ Re_x^{-\ 1/2} = -\ \psi'(0)\ .$

3. Numerical scheme and validation

Equations(7) – (10) together with the boundary conditions are numerically resolved in MATLAB employing the adaptive Runge-Kutta method [64] (for solving) and Newton Raphson (for shooting). This is accomplished by initially assuming:

$$\Xi_1 = f,\ \Xi_2 = f',\ \Xi_3 = f'',\ \Xi_3{}' = f''',$$

$$\Xi_4 = g,\ \Xi_5 = g',\ \Xi_6 = g'',\ \Xi_6{}' = g''',$$

$$\Xi_7 = \theta,\ \Xi_8 = \theta',\ \Xi_8{}' = \theta'',$$

$$\Xi_9 = \psi,\ \Xi_{10} = \psi',\ \Xi_{10}{}' = \psi''.$$

The reduced system of first-order ODE is given by:

$$\Xi_1{}' = \Xi_2,$$

$$\Xi_2{}' = \Xi_3,$$

$$\Xi_3{}' = A_1\ A_2\left\{\ (\Xi_2)^2 - \Xi_1\ \Xi_3 - A^2 - \frac{\beta}{A_2}\ \left\{(\Xi_5)^2 - \Xi_4\ \Xi_6 - 1\right\}\ \right\},$$

$$\Xi_4{}' = \Xi_5,$$

$$\Xi_5{}' = \Xi_6,$$

$$\Xi_6{}' = \frac{A_5}{\lambda}\ \{\ \Xi_4\ \Xi_3 - \Xi_1\ \Xi_6\ \},$$

$$\Xi_7{}' = \Xi_8,$$

$$\Xi_8{}' = \frac{-Pr\ \{\ A_3\ \Xi_1\ \Xi_8 + Q_T\ \Xi_7\ \}}{A_4 + \frac{4}{3}R_d},$$

$$\Xi_9{}' = \Xi_{10},$$

$$\Xi_{10}{}' = Kr\ Le\ \Xi_9 - Le\ \Xi_1\ \Xi_{10}\ .$$

with

$$\Xi_1(0) = 0,\ \Xi_2(0) = 1,\ \Xi_3(0) = \Gamma_1,\ \Xi_4(0) = 0,\ \Xi_5(0) = \Gamma_2,\ \Xi_6(0) = 0,$$

$$\Xi_7(0) = 1 + T_{slip}\ \Gamma_3,\ \Xi_8(0) = \Gamma_3,\ \Xi_9(0) = 1 + C_{slip}\ \Gamma_4,\ \Xi_{10}(0) = \Gamma_4\ .$$

where Γ_1, Γ_2, Γ_3, Γ_4 & Γ_5 are estimated using the Newton Raphson method with a suitable initial guess.

Validity of the code for the current problem has been adjudged through a restrictive correspondence of the present work with prior published works [47,62,63] (see Table 1) and a commendable agreement is noted.

4. Results and discussion

The consequence of influential parameters on velocity($f'(\eta)$), concentration($\psi(\eta)$), temperature($\theta(\eta)$), induced magnetic field($g'(\eta)$) profiles and physical quantities are illustrated via Figs. 2–25. Prandtl number(Pr) and infinity are fixed at 21 and 5, respectively. Thermophysical properties of base fluid (blood) and silver (nanoparticle) are showcased in Table 2.

Fig. 2 elucidates the positive impact of the stretching parameter (A) on $f'(\eta)$ meaning that an augmentation in stretching parameter results in the escalation of $f'(\eta)$. Fig. 3 describes the deviations in $f'(\eta)$ with β (magnetic parameter). An increase in β tends to increase $f'(\eta)$. Fig. 4 bespeaks the deviations in $f'(\eta)$ with respect to ϕ (nanoparticle volume fraction). It can be observed that $f'(\eta)$ decreases for augmenting ϕ values. This can be physically associated with the fact that ascending ϕ values, as pointed out by Mackolil and Mahanthesh [6], increases the nanofluid viscosity which in turn decreases the nanofluid velocity. The nanoparticle shape effect on velocity profile is depicted in Fig. 5. The highest nanofluid velocity profile is exhibited by cylinder-shaped silver nanoparticles followed by platelet, blade, and spherical-shaped nanoparticles, respectively.

Figs. 6 & 7 elucidate the parallel effect of β & ϕ with the differing nanoparticle shapes on $Cf_x\ Re_x^{1/2}$. It is perceived that $Cf_x\ Re_x^{1/2}$ is a decreasing function of ϕ and an increasing function of β. Further, it can be observed that the drag coefficient is highest for spherical-shaped silver nanoparticles and least for cylindrically shaped silver nanoparticles.

Fig. 8 displays the negative impact of A on $g'(\eta)$ whereas Fig. 9 displays the positive impact of β on $g'(\eta)$. A commendable agreement is noted between the results observed in Figs. 8 & 9 and the work of Ali et al. [41]. Fig. 10 explains the mixed effect of λ (reciprocal of magnetic Prandtl number) on $g'(\eta)$. Initially, elevating λ values decays $g'(\eta)$ and afterwards, a reversed trend is observed. Fig. 11 represents nanoparticle shape effect on $g'(\eta)$. The highest and lowest induced magnetic field profiles are recorded by cylindrical and spherical shaped silver nanoparticles, respectively.

The consequence of A on $\theta(\eta)$ is graphed in Fig. 12. A decline in temperature is noted for the increasing A values. Fig. 13 throws light into the constructive nature of ϕ on $\theta(\eta)$. Physically, the improvement in $\theta(\eta)$ is due to the increased thermal conductivity of fluid caused by the hike in nanoparticle volume fraction (see Mackolil and Mahanthesh [65]). In addition, the inherent nature of nanoparticles is bound to affect the temperature distribution (see Ying-Qing et al. [2] and Oke et al. [3]). The influence of Q_T (linear heat source parameter) and R_d (thermal radiation parameter) on $\theta(\eta)$ is analyzed in Figs. 14 & 15, respectively. Both parameters tend to increase $\theta(\eta)$. This can be associated with the fact that an increase in Q_T & R_d as mentioned by Mackolil and Mahanthesh [66] supplies supplemental energy to the system which triggers a surge in $\theta(\eta)$. Biologically, the increase in temperature profiles due to augmenting nanoparticle volume fraction, linear heat source, and thermal radiation unveils that the nanofluid can be used for killing tumors or cancerous cells (see Jama et al. [67]). The effect of T_{slip} (thermal slip parameter) is analyzed with the aid of Fig. 16. It is noted that augmenting T_{slip} values lead to a decrease in$\theta(\eta)$. Augmentation in the thermal slip parameter as pointed out by Sabu et al. [58] reduces the sensitivity of the fluid flow within the boundary layer, which reduces the amount of heat produced and thereby reduces the temperature. The impact of nanoparticle shape on $\theta(\eta)$ is explained in Fig. 17. The blade-shaped silver nanoparticles contribute the most towards $\theta(\eta)$ and cylinder-shaped silver nanoparticles contribute the least towards$\theta(\eta)$.

The parallel effect of ϕ, Q_T, R_d & T_{slip} with the differing nanoparticle shapes on $Nu_x\ Re_x^{-1/2}$ is elucidated in Figs. 18–21. It is seen that ϕ & R_d promotes $Nu_x\ Re_x^{-1/2}$ whereas Q_T & T_{slip} demotes $Nu_x\ Re_x^{-1/2}$. A significant rise in the heat transfer rate is showcased by the blade-shaped silver nanoparticles followed by platelet, cylinder, and spherical-shaped nanoparticles, respectively.

Variation in $\psi(\eta)$ for differing A values is demonstrated in Fig. 22 and it is perceived that A has a negative effect on$\psi(\eta)$. Fig. 23 elucidates the effect of Le (Lewis number) on$\psi(\eta)$. $\psi(\eta)$ decreases with augmenting Le values. Fig. 24 explains the negative impact of Kr (chemical reaction parameter) on $\psi(\eta)$. This can be associated with the fact that augmenting Kr values as pointed out by Neethu et al. [4] eats up the nanoparticle which decreases $\psi(\eta)$. Biologically, consumption of more nanoparticles is directly proportional to improved medication and hyperthermia (see Kaur et al. [68]). The impact of C_{slip} (solutal slip parameter) on $\psi(\eta)$ is graphed in Fig. 25. It is seen that increasing C_{slip} values help in decreasing$\psi(\eta)$. The consequence of pertinent parameters on $Sh_x\ Re_x^{-\ 1/2}$ is explained in Table 3. It is perceived that Kr & Le have a positive impact on $Sh_x\ Re_x^{-\ 1/2}$ and C_{slip} hurts $Sh_x\ Re_x^{-\ 1/2}$. In addition, it is observed that the cylinder-shaped silver nanoparticles offer the highest $Sh_x\ Re_x^{-\ 1/2}$ value.

5. Conclusion

The influence of thermal and solutal slip on the stagnation point flow of blood-based silver nanomaterial in the presence of an induced magnetic field has been examined. The significance of spherical and non-spherical silver nanoparticles on the flow profiles and physical quantities has been analyzed. The key points drawn from the study are:

- Nanofluid temperature and nanofluid concentration reduce with increasing values of thermal slip and concentration slip parameters, respectively.
- Velocity and induced magnetic field profiles are least affected by spherical-shaped silver nanoparticles and highly affected by cylinder-shaped silver nanoparticles. Blade shaped silver nanoparticles contribute the most whereas cylinder-shaped silver nanoparticles contribute the least towards the nanofluid temperature.
- Nanofluid temperature ascends with augmenting linear heat source, thermal radiation parameter, and volume fraction of silver nanoparticles.
- Blade shaped silver nanoparticles offer an increased heat transfer rate over the other nanoparticle shapes and cylinder-shaped silver nanoparticles exhibit the highest mass transfer rate. A significant rise in the surface drag is brought out by the spherical-shaped silver nanoparticles followed by blade, platelet, and cylinder-shaped nanoparticles.

CRediT authorship contribution statement

Alphonsa Mathew: Conceptualization, Data curation, Formal analysis, Methodology, Writing – original draft, Writing – review & editing. **Sujesh Areekara:** Conceptualization, Data curation, Formal analysis, Methodology, Writing – original draft, Writing – review & editing. **A.S. Sabu:** Conceptualization, Data curation, Formal analysis, Methodology, Writing – original draft, Writing – review & editing. **S. Saleem:** Writing – review & editing.

Declaration of Competing Interest

This is to certify that we the authors of the paper entitled 'Significance of multiple slip and nanoparticle shape on stagnation point flow of silver-blood nanofluid in the presence of induced magnetic field' have no conflicts of interest.

Acknowledgment

The authors acknowledge learned reviewers for their thoughtful comments and constructive suggestions. Also the authors extend their appreciation to the Deanship of Scientific Research at King Khalid University for funding this work through research groups program under Grant No. RGP.1/46/42.

References

[1] S.U.S. Choi, J.A. Eastman, Enhancing thermal conductivity of fluids with nanoparticles, Proc. 1995 Int. Mech. Eng. Congr. Expo. ASME, San Fr 66 (1995) 99–105.

[2] Y.-Q. Song, B.D. Obideyi, N.A. Shah, I.L. Animasaun, Y.M. Mahrous, J.D. Chung, Significance of haphazard motion and thermal migration of alumina and copper nanoparticles across the dynamics of water and ethylene glycol on a convectively heated surface,, Case Stud. Therm. Eng. 26 (2021), 101050, https://doi.org/10.1016/j.csite.2021.101050.

[3] A.S. Oke, I.L. Animasaun, W.N. Mutuku, M. Kimathi, N.A. Shah, S. Saleem, Significance of Coriolis force, volume fraction, and heat source/sink on the dynamics of water conveying 47 nm alumina nanoparticles over a uniform surface, Chinese J. Phys. 71 (2021) 716–727, https://doi.org/10.1016/j.cjph.2021.02.005.

[4] T.S. Neethu, S. Areekara, A. Mathew, Statistical approach on 3D hydromagnetic flow of water-based nanofluid between two vertical porous plates moving in opposite directions, Heat Transf (2021), https://doi.org/10.1002/htj.22120.

[5] R.K. Tiwari, M.K. Das, Heat transfer augmentation in a two-sided lid-driven differentially heated square cavity utilizing nanofluids, Int. J. Heat Mass Transf. 50 (2007) 2002–2018, https://doi.org/10.1016/j.ijheatmasstransfer.2006.09.034.

[6] J. Mackolil, B. Mahanthesh, Sensitivity analysis of radiative heat transfer in Casson and nano fluids under diffusion-thermo and heat absorption effects, Eur. Phys. J. Plus. 134 (2019), https://doi.org/10.1140/epjp/i2019-12949-6.

[7] Y.S. Daniel, Z.A. Aziz, Z. Ismail, F. Salah, Impact of thermal radiation on electrical MHD flow of nanofluid over nonlinear stretching sheet with variable thickness, Alexandria Eng. J. 57 (2018) 2187–2197, https://doi.org/10.1016/j.aej.2017.07.007.

[8] Y.S. Daniel, Z.A. Aziz, Z. Ismail, F. Salah, Thermal stratification effects on MHD radiative flow of nanofluid over nonlinear stretching sheet with variable thickness, J. Comput. Des. Eng. 5 (2018) 232–242, https://doi.org/10.1016/j.jcde.2017.09.001.

[9] M.N. Khan, S. Nadeem, N. Ullah, A. Saleem, Theoretical treatment of radiative Oldroyd-B nanofluid with microorganism pass an exponentially stretching sheet, Surfaces and Interfaces 21 (2020), 100686, https://doi.org/10.1016/j.surfin.2020.100686.

[10] M.N. Khan, S. Nadeem, A comparative study between linear and exponential stretching sheet with double stratification of a rotating Maxwell nanofluid flow, Surfaces and Interfaces 22 (2021), 100886, https://doi.org/10.1016/j.surfin.2020.100886.

[11] A.S. Sabu, A. Mathew, T.S. Neethu, K. Anil George, Statistical analysis of MHD convective ferro-nanofluid flow through an inclined channel with Hall current, heat source and soret effect, Therm. Sci. Eng. Prog. 22 (2021), 100816, https://doi.org/10.1016/j.tsep.2020.100816.

[12] P. Mathur, S. Jha, S. Ramteke, N.K. Jain, Pharmaceutical aspects of silver nanoparticles, Artif. Cells, Nanomed. Biotechnol. 46 (2018) 115–126, https://doi.org/10.1080/21691401.2017.1414825.

[13] R. Foulkes, M.Ali Asgari, A. Curtis, C. Hoskins, Silver-nanoparticle-mediated therapies in the treatment of pancreatic cancer, ACS Appl. Nano Mater. 2 (2019) 1758–1772, https://doi.org/10.1021/acsanm.9b00439.

[14] C. Hepokur, İ.A. Kariper, S. Mısır, E. Ay, S. Tunoğlu, M.S. Ersez, Ü. Zeybek, S. E. Kuruca, İ. Yaylım, Silver nanoparticle/capecitabine for breast cancer cell treatment, Toxicol. Vitr. 61 (2019), 104600, https://doi.org/10.1016/j.tiv.2019.104600.

[15] F.M. Abbasi, T. Hayat, B. Ahmad, Peristalsis of silver-water nanofluid in the presence of Hall and Ohmic heating effects: applications in drug delivery, J. Mol. Liq. 207 (2015) 248–255, https://doi.org/10.1016/j.molliq.2015.03.042.

[16] T. Hayat, S. Qayyum, M. Imtiaz, A. Alsaedi, Comparative study of silver and copper water nanofluids with mixed convection and nonlinear thermal radiation, Int. J. Heat Mass Transf. 102 (2016) 723–732, https://doi.org/10.1016/j.ijheatmasstransfer.2016.06.059.

[17] C.S. Sravanthi, Effect of nonlinear thermal radiation on silver and copper water nanofluid flow due to a rotating disk with variable thickness in the presence of nonuniform heat source/sink using the homotopy analysis method, Heat Transf. Res. 48 (2019) 4033–4048, https://doi.org/10.1002/htj.21581.

[18] T. Hayat, M.I. Khan, S. Qayyum, A. Alsaedi, Entropy generation in flow with silver and copper nanoparticles, Colloids Surfaces A Physicochem. Eng. Asp. 539 (2018) 335–346, https://doi.org/10.1016/j.colsurfa.2017.12.021.

[19] M. Jamiatia, Numerical investigation in comparing the influence of water-silver-magnesium oxide hybrid nanofluid and water-silver normal nanofluid on fluid flow, heat transfer and entropy generation in an enclosure with rotating heat sources, Eur. Phys. J. Plus. 134 (2019) 405, https://doi.org/10.1140/epjp/i2019-12750-7.

[20] A.A.A.A. Al-Rashed, A. Shahsavar, O. Rasooli, M.A. Moghimi, A. Karimipour, M. D. Tran, Numerical assessment into the hydrothermal and entropy generation characteristics of biological water-silver nano-fluid in a wavy walled microchannel heat sink, Int. Commun. Heat Mass Transf. 104 (2019) 118–126, https://doi.org/10.1016/j.icheatmasstransfer.2019.03.007.

[21] N.P. Truong, M.R. Whittaker, C.W. Mak, T.P. Davis, The importance of nanoparticle shape in cancer drug delivery, Expert Opin. Drug Deliv. 12 (2015) 129–142, https://doi.org/10.1517/17425247.2014.950564.

[22] E.V. Timofeeva, J.L. Routbort, D. Singh, Particle shape effects on thermophysical properties of alumina nanofluids, J. Appl. Phys. 106 (2009), https://doi.org/10.1063/1.3155999.

[23] R. Ellahi, M. Hassan, A. Zeeshan, Shape effects of spherical and nonspherical nanoparticles in mixed convection flow over a vertical stretching permeable sheet, Mech. Adv. Mater. Struct. 24 (2017) 1231–1238, https://doi.org/10.1080/15376494.2016.1232454.

[24] M. Benkhedda, T. Boufendi, T. Tayebi, A.J. Chamkha, Convective heat transfer performance of hybrid nanofluid in a horizontal pipe considering nanoparticles shapes effect, J. Therm. Anal. Calorim. 140 (2020) 411–425, https://doi.org/10.1007/s10973-019-08836-y.

[25] D. Tripathi, J. Prakash, A.K. Tiwari, R. Ellahi, Thermal, microrotation, electromagnetic field and nanoparticle shape effects on Cu-CuO/blood flow in microvascular vessels, Microvasc. Res. 132 (2020), 104065, https://doi.org/10.1016/j.mvr.2020.104065.

[26] S. Sindhu, B.J. Gireesha, Effect of nanoparticle shapes on irreversibility analysis of nanofluid in a microchannel with individual effects of radiative heat flux, velocity slip and convective heating, Heat Transf 50 (2021) 876–892, https://doi.org/10.1002/htj.21909.

[27] T. Elnaqeeb, I.L. Animasaun, N.A. Shah, Ternary-hybrid nanofluids: significance of suction and dual-stretching on three-dimensional flow of water conveying nanoparticles with various shapes and densities, Zeitschrift Für Naturforsch. A. 76 (2021) 231–243, https://doi.org/10.1515/zna-2020-0317.

[28] D.K Sembulingam, P. Sembulingam, Essentials of Medical Physiology, Sixth Edition, 2012.

[29] O.K. Koriko, I.L. Animasaun, B. Mahanthesh, S. Saleem, G. Sarojamma, R. Sivaraj, Heat transfer in the flow of blood-gold Carreau nanofluid induced by partial slip and buoyancy, Heat Transf. Res. 47 (2018) 806–823, https://doi.org/10.1002/htj.21342.

[30] A. Khalid, I. Khan, A. Khan, S. Shafie, I. Tlili, Case study of MHD blood flow in a porous medium with CNTS and thermal analysis,, Case Stud. Therm. Eng. 12 (2018) 374–380, https://doi.org/10.1016/j.csite.2018.04.004.

[31] S. Dinarvand, M.N. Rostami, R. Dinarvand, I. Pop, Improvement of drug delivery micro-circulatory system with a novel pattern of CuO-Cu/blood hybrid nanofluid flow towards a porous stretching sheet, Int. J. Numer. Methods Heat Fluid Flow. 29 (2019) 4408–4429, https://doi.org/10.1108/HFF-01-2019-0083.

[32] U. Khan, S. Bilal, A. Zaib, O.D. Makinde, A. Wakif, Numerical simulation of a nonlinear coupled differential system describing a convective flow of Casson gold–blood nanofluid through a stretched rotating rigid disk in the presence of Lorentz forces and nonlinear thermal radiation, Numer. Methods Partial Differ. Equ. (2020), https://doi.org/10.1002/num.22620.

[33] M.U. Ashraf, M. Qasim, A. Wakif, M.I. Afridi, I.L. Animasaun, A generalized differential quadrature algorithm for simulating magnetohydrodynamic peristaltic flow of blood-based nanofluid containing magnetite nanoparticles: a physiological application, Numer. Methods Partial Differ. Equ. (2020), https://doi.org/10.1002/num.22676.

[34] O.K. Koriko, K.S. Adegbie, N.A. Shah, I.L. Animasaun, M.A. Olotu, Numerical solutions of the partial differential equations for investigating the significance of partial slip due to lateral velocity and viscous dissipation: the case of blood-gold Carreau nanofluid and dusty fluid, Numer. Methods Partial Differ. Equ. (2021), https://doi.org/10.1002/num.22754.

[35] M. Kumari, H.S. Takhar, G. Nath, MHD flow and heat transfer over a stretching surface with prescribed wall temperature or heat flux, Wärme - Und Stoffübertragung 25 (1990) 331–336, https://doi.org/10.1007/BF01811556.

[36] F.M. Ali, R. Nazar, N.M. Arifin, I. Pop, MHD boundary layer flow and heat transfer over a stretching sheet with induced magnetic field, Heat Mass Transf. 47 (2011) 155–162, https://doi.org/10.1007/s00231-010-0693-4.

[37] M. Saleem Iqbal, F. Malik, I. Mustafa, I. Khan, A. Ghaffari, A. Riaz, K. Sooppy Nisar, Impact of induced magnetic field on thermal enhancement in gravity driven Fe_3O_4 ferrofluid flow through vertical non-isothermal surface, Results Phys 19 (2020), 103472, https://doi.org/10.1016/j.rinp.2020.103472.

[38] B.J. Gireesha, B. Mahanthesh, I.S. Shivakumara, K.M. Eshwarappa, Melting heat transfer in boundary layer stagnation-point flow of nanofluid toward a stretching sheet with induced magnetic field, Eng. Sci. Technol. an Int. J. 19 (2016) 313–321, https://doi.org/10.1016/j.jestch.2015.07.012.

[39] Z. Iqbal, E.N. Maraj, E. Azhar, Z. Mehmood, Framing the performance of induced magnetic field and entropy generation on Cu and TiO_2 nanoparticles by using Keller box scheme, Adv. Powder Technol. 28 (2017) 2332–2345, https://doi.org/10.1016/j.apt.2017.06.015.

[40] M. Amjad, I. Zehra, S. Nadeem, N. Abbas, A. Saleem, A. Issakhov, Influence of Lorentz force and induced magnetic field effects on Casson micropolar nanofluid flow over a permeable curved stretching/shrinking surface under the stagnation region, Surfaces and Interfaces 21 (2020), 100766, https://doi.org/10.1016/j.surfin.2020.100766.

[41] F.M. Ali, R. Nazar, N.M. Arifin, I. Pop, MHD stagnation-point flow and heat transfer towards stretching sheet with induced magnetic field, Appl. Math. Mech. - English Ed. 32 (2011) 409–418, https://doi.org/10.1007/s10483-011-1426-6.

[42] T.R. Mahapatra, A.S. Gupta, Heat transfer in stagnation-point flow towards a stretching sheet, Heat Mass Transf 38 (2002) 517–521, https://doi.org/10.1007/s002310100215.

[43] M.M. Junoh, F.M. Ali, N.M. Arifin, N. Bachok, I. Pop, MHD stagnation-point flow and heat transfer past a stretching/shrinking sheet in a hybrid nanofluid with induced magnetic field, Int. J. Numer. Methods Heat Fluid Flow. 30 (2019) 1345–1364, https://doi.org/10.1108/HFF-06-2019-0500.

[44] N. Abbas, M.Y. Malik, M.S. Alqarni, S. Nadeem, Study of three dimensional stagnation point flow of hybrid nanofluid over an isotropic slip surface, Phys. A Stat. Mech. Its Appl. 554 (2020), 124020, https://doi.org/10.1016/j.physa.2019.124020.

[45] F. Al-Amri, M. Muthtamilselvan, Stagnation point flow of nanofluid containing micro-organisms,, Case Stud. Therm. Eng. 21 (2020), 100656, https://doi.org/10.1016/j.csite.2020.100656.

[46] R. Ul Haq, S. Nadeem, Z.H. Khan, N.S. Akbar, Thermal radiation and slip effects on MHD stagnation point flow of nanofluid over a stretching sheet, Phys. E Low-Dimensional Syst. Nanostructures. 65 (2015) 17–23, https://doi.org/10.1016/j.physe.2014.07.013.

[47] Z. Iqbal, E. Azhar, E.N. Maraj, Transport phenomena of carbon nanotubes and bioconvection nanoparticles on stagnation point flow in presence of induced magnetic field, Phys. E Low-Dimensional Syst. Nanostructures. 91 (2017) 128–135, https://doi.org/10.1016/j.physe.2017.04.022.

[48] M. Abd El-Aziz, A.A. Afify, Influences of slip velocity and induced magnetic field on MHD stagnation-point flow and heat transfer of casson fluid over a stretching sheet, Math. Probl. Eng. (2018), 9402836, https://doi.org/10.1155/2018/9402836.

[49] M.I. Khan, T. Hayat, F. Shah, F.Haq Mujeeb-Ur-Rahman, Physical aspects of CNTs and induced magnetic flux in stagnation point flow with quartic chemical reaction, Int. J. Heat Mass Transf. 135 (2019) 561–568, https://doi.org/10.1016/j.ijheatmasstransfer.2019.01.141.

[50] Y.S. Daniel, Z.A. Aziz, Z. Ismail, F. Salah, Effects of slip and convective conditions on MHD flow of nanofluid over a porous nonlinear stretching/shrinking sheet, Aust. J. Mech. Eng. 16 (2018) 213–229, https://doi.org/10.1080/14484846.2017.1358844.

[51] S.A. Khan, Y. Nie, B. Ali, Multiple slip effects on MHD unsteady viscoelastic nano-fluid flow over a permeable stretching sheet with radiation using the finite element method, SN Appl. Sci. 2 (2019) 66, https://doi.org/10.1007/s42452-019-1831-3.

[52] C.H. Amanulla, S. Saleem, A. Wakif, M.M. AlQarni, MHD Prandtl fluid flow past an isothermal permeable sphere with slip effects,, Case Stud. Therm. Eng. 14 (2019), 100447, https://doi.org/10.1016/j.csite.2019.100447.

[53] W. Ibrahim, M. Negera, MHD slip flow of upper-convected Maxwell nanofluid over a stretching sheet with chemical reaction, J. Egypt. Math. Soc. 28 (2020) 7, https://doi.org/10.1186/s42787-019-0057-2.

[54] A.K. Barik, S.K. Mishra, S.R. Mishra, P.K. Pattnaik, Multiple slip effects on MHD nanofluid flow over an inclined, radiative, and chemically reacting stretching sheet by means of FDM, Heat Transf. Res. 49 (2020) 477–501, https://doi.org/10.1002/htj.21622.

[55] Y. Daniel, MHD Laminar flows and heat transfer adjacent to permeable stretching sheets with partial slip condition, J. Adv. Mech. Eng. 4 (2017), https://doi.org/10.7726/jame.2017.1001.

[56] Y.S. Daniel, Z.A. Aziz, Z. Ismail, F. Salah, Hydromagnetic slip flow of nanofluid with thermal stratification and convective heating, Aust. J. Mech. Eng. 18 (2020) 147–155, https://doi.org/10.1080/14484846.2018.1432330.

[57] Y.S. Daniel, Z.A. Aziz, Z. Ismail, A. Bahar, F. Salah, Slip role for unsteady MHD mixed convection of nanofluid over stretching sheet with thermal radiation and electric field, Indian J. Phys. 94 (2020) 195–207, https://doi.org/10.1007/s12648-019-01474-y.

[58] A.S. Sabu, S. Areekara, A. Mathew, Effects of multislip and distinct heat source on MHD Carreau nanofluid flow past an elongating cylinder using the statistical method, Heat Transf (2021), https://doi.org/10.1002/htj.22142.

[59] B. Ankamwar, Size and shape effect on biomedical applications of nanomaterials. Biomed. Eng. - Tech. Appl. Med., IntechOpen, Rijeka, 2012, https://doi.org/10.5772/46121.

[60] H. Chugh, D. Sood, I. Chandra, V. Tomar, G. Dhawan, R. Chandra, Role of gold and silver nanoparticles in cancer nano-medicine, Artif. Cells, Nanomedicine, Biotechnol 46 (2018) 1210–1220, https://doi.org/10.1080/21691401.2018.1449118.

[61] H. Farrokhi, D.O. Otuya, A. Khimchenko, J. Dong, Magnetohydrodynamics in Biomedical Applications. Nanofluid Flow Porous Media, 2019, https://doi.org/10.5772/intechopen.87109.

[62] T. Hayat, M. Farooq, A. Alsaedi, Homogeneous-heterogeneous reactions in the stagnation point flow of carbon nanotubes with Newtonian heating, AIP Adv 5 (2015) 27130, https://doi.org/10.1063/1.4908602.

[63] T. Hayat, K. Muhammad, M. Farooq, A. Alsaedi, Melting heat transfer in stagnation point flow of carbon nanotubes towards variable thickness surface, AIP Adv 6 (2016) 15214, https://doi.org/10.1063/1.4940932.

[64] J. Kiusalaas, Numerical Methods in Engineering with MATLAB®, Cambridge University Press, Cambridge, 2005 https://doi.org/10.1017/CBO9780511614682.

[65] J. Mackolil, B. Mahanthesh, Heat transfer enhancement using temperature-dependent effective properties of alumina-water nanoliquid with thermo-solutal Marangoni convection: a sensitivity analysis, Appl. Nanosci. (2021), https://doi.org/10.1007/s13204-020-01631-4.
[66] J. Mackolil, B. Mahanthesh, Inclined magnetic field and nanoparticle aggregation effects on thermal Marangoni convection in nanoliquid: a sensitivity analysis, Chinese J. Phys. 69 (2021) 24–37, https://doi.org/10.1016/j.cjph.2020.11.006.
[67] M. Jama, T. Singh, S.M. Gamaleldin, M. Koc, A. Samara, R.J. Isaifan, M.A. Atieh, Critical review on nanofluids: preparation, characterization, and applications, J. Nanomater. (2016), 6717624, https://doi.org/10.1155/2016/6717624.
[68] P. Kaur, M.L. Aliru, A.S. Chadha, A. Asea, S. Krishnan, Hyperthermia using nanoparticles – promises and pitfalls, Int. J. Hyperth. 32 (2016) 76–88, https://doi.org/10.3109/02656736.2015.1120889.